ISSN 1995-0802, Lobachevskii Journal of Mathematics, 2023, Vol. 44, No. 10, pp. 4457–4468. © Pleiades Publishing, Ltd., 2023.

Effect of Temperature Distribution on the Calculation of the Thermal Current in the Mathematical Model of Pulsed Heating of a Tungsten

G. G. Lazareva[1*] and V. A. Popov[2,3]**

(Submitted by A. B. Muravnik)

[1] *Peoples Friendship University of Russia (RUDN University), Moscow, 117198 Russia*

[2] *Budker Institute of Nuclear Physics of Siberian Branch, Russian Academy of Sciences (BINP SB RAS), Novosibirsk, 630090 Russia*

[3] *Federal State Autonomous Educational Institution of Higher Education "Novosibirsk National Research State University," Novosibirsk, 630090 Russia*

Received June 7, 2023; revised July 20, 2023; accepted July 31, 2023

Abstract—In this paper current distribution model in the tungsten sample and vapor at surface under electron beam heat was considered. The model is based on the solutions of electrodynamic equations and the two-phase Stefan problem in cylindrical coordinates. The two-phase Stefan problem defines the temperature inside a sample area taking into account the evaporation at its surface. A model temperature distribution in a thin layer of evaporated tungsten is used, which repeats the surface temperature. The electrodynamic equation include received temperature values and solved over the whole region. The case of constant values of electrical resistance and thermoemf in gases and metals is considered. The temperature calculations were made considering constant coefficients and temperature dependencies of specific heat capacity, density and thermal conductivity. It is shown that the detail of the coefficients of the Stefan problem has a great influence on the results of solving the electrodynamics equation. The model parameters are taken from the experiments on the Beam of Electrons for materials Test Applications (BETA) stand, created at the BINP SB RAS.

DOI: 10.1134/S199508022310027X

Keywords and phrases: *mathematical modeling, thermal currents, tungsten, pulse heating, successive over-relaxation, beta stand, divertor material.*

1. INTRODUCTION

The experimental stand Beam of Electrons for Materials Test Applications (BETA) created at the Budker Institute of Nuclear Physics SB RAS [1], has yielded new experimental data on the erosion of the surface of a tungsten sample under impulse action of an electron beam. The full-scale experiment is constantly accompanied by a numerical simulation [2]. The tungsten heating model is based on solving the equations of electrodynamics and the two-phase Stefan problem for temperature in the region of the sample [3]. The condition on a free boundary molten—solid body consists of the temperature continuity and discontinuity of the heat flow due to the absorption or release of a heat. The position and velocity of the free boundary depends on the coefficients: specific heat capacity, density and thermal conductivity of tungsten. In the case of constant coefficients, the temperature on the surface is a smooth function. If coefficients in the form of dependencies on temperature are used in the calculation, then the solution for the Stefan problem has small peculiarities. The work let's into the calculation of the current in the sample for these two cases. The influence of temperature inhomogeneity on the current strength is being investigated in the presence of significant influences on the current generation, such as the difference in electrical resistance and thermoelectric effects in the metal and its vapors. An electromotive force arises in regions with variations in material parameters. It is important to note that the electromotive force

[*] E-mail: lazareva-gg@rudn.ru

[**] E-mail: v.a.popov94@gmail.com

differs in gases and melts. Therefore, a non-zero accelerating voltage arises across the closed circuit through the gas and the melt, which generates a current along this circuit. The current, interacting with the magnetic field, causes the overall movement of the substance. This work considers the case where equations for fields and currents are formulated for a tungsten sample in a cylindrical coordinate system, considering the electromotive forces arising in the gas above the sample [4]. It is assumed that the characteristic time of change is large compared to the time required for the equilibrium of the electromagnetic equations to be established on the scale of the problem. Further development of the model involves refining the calculation of the gas's specific electrical conductivity and thermoelectric effects, considering the dependence of these parameters on gas density. The calculation results by means of the final models are used for comparison with the experimental data obtained at the BETA experimental stand. The article consists of the problem definition (temperature recovery and themlal current determination), the solution method for the Stefan problem and for the current distribution, the analysis of the Computation results.

2. PROBLEM DEFINITION

In the experiments on the BETA stand, samples of rolled tungsten were exposed to an axisymmetric electron beam [5]. Electrons with an energy of 80−90 keV heat the material in a layer thin as compared with the characteristic depth of heating of the material. The heat absorbed by the surface propagates into the material. A sample has dimensions of 25 mm × 25 mm and a thickness of 4 mm. Since in such a short time the sample is heated to a depth of several hundred microns, the simulation region was a transverse section of the sample (sample thickness 3 mm) and a thin vapor layer (layer thickness 3 mm), a region of 12 mm × 6 mm. The numerical model for the distribution of beam current in the heated sample and tungsten vapors is simplified to solving a combined system of Maxwell's equations and the Stefan problem.

2.1. Temperature Recovery

Consider the following heat equation with surface heating

$$\begin{cases} lc(T)\rho(T)\frac{\partial T}{\partial t} = \frac{1}{r}\frac{\partial}{\partial r} r\lambda(T)\frac{\partial T}{\partial r} + \frac{\rho(T)}{\rho_0}\frac{\partial}{\partial z}\frac{\rho(T)}{\rho_0}\lambda(T)\frac{\partial T}{\partial z}, \\ (n, \nabla T)|_\gamma = \frac{W(t,r)-N(t,r)}{\lambda(T)}, \\ (n, \nabla T) = 0 \quad \text{at other boundaries}, \\ T|_{t=0} = T_0, \\ \left[\lambda(T)\frac{\partial T}{\partial t}\right]\Big|_\Gamma = L_m v_n, \quad [T]|_\Gamma = 0, \end{cases} \tag{1}$$

where $T(r, z, t)$ is the temperature, $c(T)$ is the specific heat, $\rho(T)$ is the density, $\rho_0 = \rho(T_0)$ is the density at the initial moment, $\lambda(T)$ is the thermal conductivity, $W(t, r) = 2 \times 10^4$ W/mm^2 is the distribution of power over the surface of the heat flux γ, $N(t, r)$ is the evaporation power on the surface, n is the normal to the surface, $T_0 = 300$ K is the initial temperature, Γ is the free boundary, L_m is the enthalpy of the phase transition, v_n is the velocity of the free boundary. $T_m = 3695$ K is a melting temperature. Phase transitions inherent in the considered problem are included in the coefficients of equation (1). Density (see Fig. 2a), thermal conductivity (see Fig. 2b), specific heat capacity (see Fig. 2c), and evaporation power (see Fig. 2d) are shown as dependencies on material temperature up to 8000 K. These functions have discontinuities or lose smoothness at the melting point T_m;

$$\rho(T) = \begin{cases} 1.94 \times 10^{-4} - 2.67 \times 10^{-10}T + 4.74 \times 10^{-15}T^2 - 9.52 \times 10^{-18}T^3, & T_0 \le T \le T_m, \\ 16.27 \times 10^{-6} - 7.68 \times 10^{-10}(T - T_m) - 8.09 \times 10^{-14}(T - T_m)^2, & T_m < T \le 8000, \end{cases}$$

$$c(T) = \begin{cases} 1.2 \times 10^{-4} + 4.34 \times 10^{-8}T - 2.02 \times 10^{-14}T^2 + 5.8 \times 10^{-15}T^3 + \\ 7.53 \times 10^{-8}T^4, \quad T_0 \le T < 3080, \\ 1.1 \times 10^{-5} + 6.45 \times 10^{-8}T, \quad 3080 \le T < T_m, \\ 2.76 \times 10^{-4}, \quad T_m \le T \le 8000; \end{cases}$$

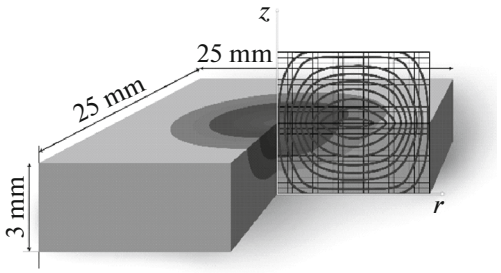

Fig. 1. Scheme of the experiment. An axially symmetric electron beam in a leading coaxial magnetic field is incident on the sample along the normal (beem at the figure falls from above, doesn't plotted). The temperature distribution is schematically indicated by color. The insert shows the distribution of induced currents.

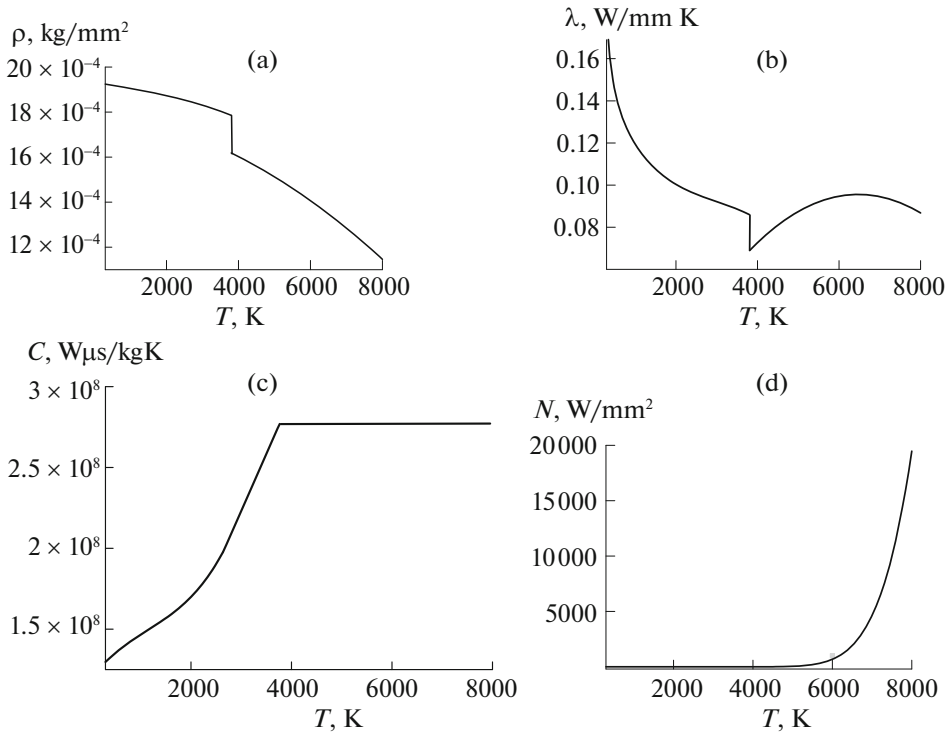

Fig. 2. Graphs of temperature dependencies of (a) density, (b) thermal conductivity, (c) specific heat, and (d) power loss for evaporation.

$$\lambda(T) = \begin{cases} 149.44 \times 10^{-3} - 45.47 \times 10^{-6}T + 13.2 \times 10^{-9}T^2 - 1.48 \times 10^{-12}T^3 + \\ 3.87 \times 10^{3}T^{-2}, \quad T_0 \le T < T_m, \\ -12.76 \times 10^{-3} + 27.74 \times 10^{-6}T - 1.65 \times 10^{-9}T^2, \quad T_m \le T \le 8000. \end{cases}$$

Measuring the thermophysical characteristics of refractory metals is a difficult task. Many reference books and articles give an approximate or theoretically predicted dependence with an accuracy estimate of 10 % and worse. The thermal conductivity and heat capacity of solid tungsten are taken from [6]. The estimates for the thermal conductivity of liquid tungsten are taken from [7, 8]. It is necessary to choose the function $\lambda(T)$ at large temperature values such that there is no division by zero.

It is more convenient to proceed in non-dimensional variables, for example, as follows (Table 1)

$$r^* = \frac{r}{r_0}, \quad \lambda^* = \frac{\lambda}{\lambda_0}, \quad \rho^* = \frac{\rho}{\rho_0}, \quad c^* = \frac{c}{c_0}, \quad t^* = \frac{\lambda_0 t}{\rho_0 c_0 {r_0}^2}, \quad T^* = \frac{T}{T_0}, \quad W^* = \frac{\lambda_0 T_0 W}{r_0}.$$

Table 1. The characteristic values of the parameters

Parameter	Typical value	Units
r_0	1	mm
t_0	10^2	μ s
λ_0	10^{-1}	W/(mm K)
ρ_0	10^{-5}	kg/mm^3
c_0	10^8	W μ s/(kg K)
T_0	10^3	K
W_0	10^3	W/mm^2
I_0	10^3	A
j_0	10^3	A/mm^2
S_0	10^{-2}	V/K
ρ_{e0}	10^{-2}	V mm/A

The calculations are based on available data on the temperature gradient of evaporating tungsten above the surface [9, 10]. The calculations were carried out under the assumption that the gas temperature remains constant when considering a 3 mm gas layer above the surface. The obtained relationship between temperature and radius, resulting from solving Stefan's problem, remains consistent with existing data. Thus, the temperature of the gas T_{gas} is equal to the temperature of the surface $T|_\gamma$ of the plate: $T_{gas}(r,z) = T(r)|_\gamma$. Existing developments allow for the calculation of gas temperature and density from a system of gas dynamics equations, which will be utilized in further expanding the model. The objective of this study is to investigate the influence of the coefficients of the system (1) on the calculation of heat fluxes in the sample and in the thin vapor layer above it.

2.2. Themlal Current Determination

The process of current propagation in the sample can be considered stationary since the characteristic time of change is large as compared to the time of establishing equilibrium of the equations of electrodynamics on the scale of the problem [11]. The current distribution is calculated at the time when the sample is heated up to the maximum temperature. Taking the evaporation process into account ensures that the temperature increase is limited in the sample, which corresponds to the experimental data [2]. The system of Maxwell equations for calculating the current in the sample is modified for the stationary case in the cylindrical coordinate system

$$\begin{cases} \nabla \times \vec{B} = \frac{4\pi}{c}\vec{j}, \\ \nabla \times \vec{E} = 0, \quad \nabla \cdot \vec{B} = 0, \\ \nabla \cdot \vec{j} = 0, \quad \vec{E} = \rho_e \vec{j}, \end{cases} \tag{2}$$

where ρ_e is the specific conductivity, $\vec{B}$ is the magnetic field, $\vec{E} = E(E_r, E_\varphi, E_z)$ is the electric field and $\vec{j} = (J_r, j_\varphi, j_z)$ is the current. We introduce the vector potential of the current $F = (F_r, F_\varphi, F_z)$:

$$\vec{j} = \nabla \times \vec{F} \tag{3}$$

and write (2) in the cylindrical coordinate system (r, φ, z). Note that the derivatives with respect to the angle φ will be zero due to the symmetry of the problem with respect to rotation [12, 13]. We express the current in terms of the vector potential of the current taking into consideration the zero derivative with respect to the angle. Since a vortex electric field is absent, the current flows only in the axial and radial

directions, and $E_\varphi = 0$. It follows that $j_\varphi = 0$:

$$\vec{j} = \begin{pmatrix} j_r \\ j_\varphi \\ j_z \end{pmatrix} = \begin{pmatrix} \frac{1}{r}\frac{\partial F_z}{\partial \varphi} - \frac{\partial F_\varphi}{\partial z} \\ \frac{\partial F_r}{\partial z} - \frac{\partial F_z}{\partial r} \\ \frac{1}{r}\frac{\partial r F_\varphi}{\partial r} - \frac{1}{r}\frac{\partial F_r}{\partial \varphi} \end{pmatrix} = \begin{pmatrix} -\frac{\partial F_\varphi}{\partial z} \\ 0 \\ \frac{1}{r}\frac{\partial r F_\varphi}{\partial r} \end{pmatrix}.$$

Thus, to describe the current, it suffices to use only one function F_φ describing the "vorticity" of the current. Taking into account the zero derivative with respect to the angle φ and the absence of a vortex electric field $j_\varphi = 0$, the generalized Ohm's law can be expressed as follows

$$\vec{j} = \left(\vec{E} - S\nabla T - \nabla\mu/e\right)/\rho_e.$$

The equation for "vorticity" for a single nontrivial component is obtained. Here, μ represents the chemical potential of electrons, and e represents the charge of an electron. To achieve this, the vector operator "curl" (rot) is applied to both sides of equation (3)

$$\nabla \times \left(\rho_e \vec{j}\right) = \nabla \times \left(\vec{E} - S\nabla T - \nabla\mu/e\right) = \nabla \times (S\nabla T) = \nabla S \times \nabla T.$$

The expression is greatly simplified due to the potential nature of the electric field and the chemical potential. Similarly to the previously discussed case for heat fluxes in the sample [3], for equation (2), the following expression is obtained

$$\frac{\partial^2 F_\varphi}{\partial r^2} + \frac{\partial^2 F_\varphi}{\partial z^2} + \frac{\partial F_\varphi}{\partial r}\left(\frac{1}{\rho_e}\frac{\partial \rho_e}{\partial r} + \frac{1}{r}\right) + \frac{\partial F_\varphi}{\partial z}\frac{1}{\rho_e}\frac{\partial \rho_e}{\partial z}$$
$$+F_\varphi\left(\frac{1}{r\rho_e}\frac{\partial \rho_e}{\partial r} + \frac{1}{r^2}\right) = \frac{1}{\rho_e}\left(\frac{\partial S}{\partial r}\frac{\partial T}{\partial z} - \frac{\partial S}{\partial z}\frac{\partial T}{\partial r}\right).$$

After introducing the total current $I(r,z) = 2\pi r F_\varphi$, the equation takes the following form

$$\frac{\partial^2 I}{\partial r^2} + \frac{\partial^2 I}{\partial z^2} + \frac{\partial I}{\partial r}\frac{\partial \ln(\rho_e/r)}{\partial r} + \frac{\partial I}{\partial z}\frac{\partial \ln(\rho_e/r)}{\partial z} = \frac{2\pi r}{\rho_e}\left(\frac{\partial S}{\partial r}\frac{\partial T}{\partial z} - \frac{\partial S}{\partial z}\frac{\partial T}{\partial r}\right). \tag{4}$$

Denoting $\Phi = \ln(\rho_e/r)$ and using ∇ as the differential operator in the orthogonal coordinate system (r,z), the problem can be written as follows

$$\begin{cases} \rho_e \nabla^2 I + \rho_e \nabla I \nabla \Phi = 2\pi r \nabla S \nabla T, \quad 0 < r < r_{\max}, \quad 0 < z < z_{\max}, \quad 0 < t, \\ \Phi = \ln(\rho_e/r), \quad I|_{t=0} = 0, \\ I|_{(0,z)} = 0, \quad \frac{\partial I}{\partial n}\big|_{(r_{\max},z)} = 0, \quad \frac{\partial I}{\partial n}\big|_{(r,z_{\max})} = 0, \quad I|_{(r,0)} = 0. \end{cases} \tag{5}$$

In the calculation of currents without considering the evaporating gas [3], the boundary conditions played a crucial role in determining the currents. In the initial-boundary problem (5), the solution is determined by the right-hand side of the equation, as the considered domain contains current sources due to thermionic emission. Homogeneous Dirichlet boundary conditions for the current in the sample and the gas above the sample simplify numerical calculations. Undoubtedly, such a choice of boundary conditions is not exact, but the accuracy of this approximation can be improved by increasing the computational domain. This does not contradict the problem formulation since in the modeled experiment, the sample is fixed in a setup with a large internal diameter (10 cm) filled with a high vacuum. The formulation of problem (5) allows us to avoid determining the current at the boundary of the evaporating gas. The calculation of thermionic emission comes to the forefront. The characteristic parameter values are provided in Table 1.

3. SOLUTION METHOD

3.1. Solution Method for the Stefan Problem

To incorporate the conditions at the boundary between the melt and the solid phase, the differential equation itself has been modified in the context of continuum schemes [14, 15]. In Equation (1), a term appears in the multiplier of the time derivative, which contains the latent heat of fusion $L_m = 51.1 \times 10^5 \frac{\mathrm{W}\mu\mathrm{s}}{\mathrm{mm}^3}$ acting within the smoothing interval

$$(c(T)\rho(T) + L_m\delta(T,\Delta))\frac{\partial T}{\partial t} = \frac{1}{r}\frac{\partial}{\partial r}r\lambda(T)\frac{\partial T}{\partial r} + \frac{\rho^*(T)}{\rho_0}\frac{\partial}{\partial z}\frac{\rho^*(T)}{\rho_0}\lambda(T)\frac{\partial T}{\partial z}.$$

The multiplier $\delta(T,\varepsilon)$ acts on a narrow smoothing interval $[-\varepsilon,\varepsilon]$, $\varepsilon = 5$ K around the melting temperature $T_m = 3695$ K and is calculated as follows

$$\delta(T,\varepsilon) = \begin{cases} \frac{1}{2\varepsilon}, & |T - T_m| \le \varepsilon, \\ 0, & |T - T_m| > \varepsilon. \end{cases}$$

A uniform rectangular grid with nodes $(i,k) : i = 1 \dots N_r, k = 1 \dots N_z$ is introduced in the two-dimensional domain $(r,z) : r \in [r_0, r_{\max}], z \in [z_0, z_{\max}], r_0 = z_0 = 0, r_{\max} = 12$ mm, $z_0 = 3$ mm. The plates used are squares approximately 25 mm $\times$ 25 mm and 3 mm thick. The size of the computational domain corresponds to the dimensions of the samples, but the problem formulation in cylindrical geometry assumes the consideration of a plate in the form of a puck. Such an assumption does not have a significant impact on the results since the power distribution over the surface of the heat flux has maximum values at the center of the sample and decreases proportionally with the radius. The heating of the sample occurs in the center of the plate and does not reach its edges. The sample is heated to a depth not exceeding 1 mm. Thus, the main focus during the calculation should be given to the boundary conditions on the heated surface and along the axis of symmetry. Boundary conditions at heated surface $\frac{\partial T}{\partial z}\big|_{z=0} = \frac{W(t,r)-N(t,r)}{\lambda(T)}$ depends on three non-linear coefficients. The power distribution over the heat flow surface is given by the following equation $W(t,r) = W_{\max}(t)\exp(-Ar^2)$. Here $A = 1/a^2 = 0.03088523$ 1/mm^2 is a constant characterizing the beam radius a, which has the same value for each series of experiments and is used to calculate the boundary condition for problem (2), $W_{\max}(t) = 2 \times 10^4$ W/mm^2. The heating power density distribution over the surface was measured using X-ray imaging [6]. Power loss for the evaporation process $N(T|_\gamma) = L_e \cdot \frac{1}{S}\frac{dm}{dt}$, where $\frac{1}{S}\frac{dm}{dt}$ is mass evaporation rate, L_e is evaporation enthalpy. Power loss is calculated using the following equations

$$L_e = 4.482 \times 10^{12}\frac{\mathrm{W}\mu\mathrm{s}}{\mathrm{kg}}, \quad \frac{1}{S}\frac{dm}{dt} = P(T|_\gamma)\sqrt{\frac{M}{2\pi R T|_\gamma}}$$

$$= \exp\left(26.19104 - \frac{83971.3\ \mathrm{K}}{T|_\gamma}\right)\sqrt{\frac{0.184\ \mathrm{K}}{2\pi 8.314 T|_\gamma}}10^{-12}\frac{\mathrm{kg}}{\mathrm{mm}^2\,\mu\mathrm{s}}.$$

Here $T|_\gamma$ is temperature at surface, $P(T|_\gamma)$ is saturated steam pressure. The derivation of the power loss equation and the justification for neglecting temperature radiation by the surface in the energy balance are presented in more detail in the study [16]. Let's define on a grid with nodes $t^n = n\tau$, $n = 1, \dots, T$, $r_i = ih$, $i = 1, \dots, N_r$, $z_k = kh$, $k = 1, \dots, N_z$ grid functions

$$T^n_{ik} = T(t^n, r_i, z_k), \quad C^n_{ik} = c(T^n_{ik})\rho(T^n_{ik}) + L_m\delta(T^n_{ik},\Delta), \quad R^n_{ik} = \frac{\rho^*(T^n_{ik})}{\rho_0}, \quad L^n_{ik} = \lambda(T^n_{ik}).$$

On the heated surface the boundary conditions is set with the use of node functions

$$W^n_i = W_{\max}(t^n)\exp(-Ar_i{}^2), \quad N^n_i = N(t^n, r_i).$$

Initial conditions: $T^o_{ik} = T_0$. Difference operators are introduced

$$(\Lambda_{rr})^n_{ik} = \frac{1}{r_i h^2 C^n_{ik}}\left[r_{i+1/2}L^n_{ik}\left(T^n_{i+1k} - T^n_{ik}\right) - r_{i-1/2}L^n_{ik}\left(T^n_{ik} - T^n_{i-1k}\right)\right],$$

$$(\Lambda_{zz})^n_{ik} = \frac{R^n_{ik}}{h^2 C^n_{ik}} \left[R^n_{ik+1/2} L^n_{ik+1/2} \left(T^{n1}_{ik+1} - T^n_{ik} \right) \right],$$
$$f_{i+1/2j} = \frac{f_{ij} + f_{i+1j}}{2}, \quad f_{ij+1/2} = \frac{f_{ij} + f_{ij+1}}{2}. \tag{6}$$

The calculation of temperature at internal points of the computational domain is implemented using the Douglas–Rachford method and tridiagonal matrix algorithm [17]. The coefficients are computed based on the temperature values from the previous layer. The finite difference scheme for the equation (1) has the following form

$$\begin{cases} \frac{T^{n+1/2}_{ik} - T^n_{ik}}{\tau} = (\Lambda_{rr})^{n+1/2}_{ik} + (\Lambda_{zz})^n_{ik}, \\ \frac{T^{n+1}_{ik} - T^{n+1/2}_{ik}}{\tau} = (\Lambda_{zz})^{n+1}_{ik} - (\Lambda_{zz})^n_{ik}. \end{cases}$$

The boundary conditions at each stage have the form

$$\frac{T^{n+1/2}_{N_r-2,k} - 4T^{n+1/2}_{N_r,k} + 3T^{n+1/2}_{N_r-1,k}}{2h} = 0,$$
$$\frac{T^{n+1/2}_{2k} - T^{n+1/2}_{1k}}{h} - \frac{h}{4L^n_{1k}} \left\{ C^n_{1k} \frac{T^{n+1/2}_{2k} - T^n_{2k}}{\tau} + (\Lambda_{zz})^{n+1/2}_{1k} \right\} = 0,$$
$$\frac{T^{n+1}_{i,3} - 4T^{n+1}_{i,2} + 3T^{n+1}_{i,1}}{2h} = \frac{W^{n+1}_i - N^{n+1}_i}{L^{n+1}_{i1}}, \quad \frac{T^{n+1}_{i,N_z-2} - 4T^{n+1}_{i,N_z} + 3T^{n+1}_{i,N_z-1}}{2h} = 0.$$

The proposed solution scheme has a second-order spatial approximation and eliminates the need to specify the phase transformation boundary. Equation (1) has a divergent form, which allows for the use of conservative schemes. The solution of the system (6) with constant coefficients has been tested against known analytical solutions, while the solution with variable coefficients has been tested against experimental data. It is known that heating a tungsten sample with a power density of 10^3 W/mm^2 for 1000 μs results in the sample reaching a temperature of 20000 K. Interesting results from the calculations in [2] demonstrated a complete match between the dynamics of the computed and experimental melt radius when considering evaporation at the boundary of the tungsten plate. The proposed algorithm is cost-effective and straightforward to implement, and it can be used for simulating the melting of other refractory metals. It is possible that using iterative methods [18] to implement such an approach would be more efficient.

3.2. Solution Method for the Current Distribution

The problem was previously solved only in the sample region [3]. Currently, it is impossible to solve the problem solely in the vapor region because the boundary condition formulation for heat flows in the gas above the metal surface poses significant challenges. In the considered formulation, the issue of boundary condition formulation is resolved, but a number of difficulties arise. The current amplitude cannot be accurately determined for a continuous problem with any degree of simplification because the derivatives at the discontinuity point take on an infinite value. Without regularization, it is not possible to proceed with the numerical solution of the problem, as it may lead to a solution dependent on the step size h of the computational grid.

To use continuous approximation schemes and account for the conditions at the boundary between the plate material and the vapor, it is necessary to transform Eq. (4). In the term $\frac{\partial I}{\partial z} \frac{\partial \ln(\rho_e/r)}{\partial z}$, both factors experience a discontinuity at the sample surface. The derivative of the current with respect to the surface normal changes sign because the currents reach a maximum at the metal-gas boundary. However, the solution of Eq. (4) has positive second derivatives everywhere outside the sample surface. The derivative with respect to the surface normal of the specific conductivity is a derivative of the discontinuous function, as the specific conductivity of the metal is two orders of magnitude higher than that of the gas, regardless of the method used to determine it. Similarly, the term $\frac{\partial S}{\partial z} \frac{\partial T}{\partial r}$ in the right-hand side of Eq. (4) contains a derivative of the discontinuous thermoelectric power function.

Derivatives with respect to z of the discontinuous functions are calculated using the Dirac delta function. The proposed replacement [19] of the derivative at the discontinuity point with a continuous function $\delta(z-z_0)$, multiplied by the jump in thermoelectric power over the interval $[z_0-2h, z_0+2h]$, is adapted to the problem under consideration. After regularization, the right-hand side of Equation (4) takes the following form

$$\frac{\partial^2 I}{\partial r^2}+\frac{\partial^2 I}{\partial z^2}+\frac{\partial I}{\partial r}\frac{\partial \ln(\rho_e/r)}{\partial r}+\frac{\partial I}{\partial z}\frac{\partial \ln(\rho_e/r)}{\partial z}$$
$$=\frac{2\pi r}{\rho_e}\left(\frac{\partial S}{\partial r}\frac{\partial T}{\partial z}-\frac{\partial T}{\partial r}\left\{\left(\frac{\partial S}{\partial z}\right)_{z\neq z_0}+\delta(z-z_0)[S]_{z=z_0}\right\}\right).$$

Since the derivative $\frac{\partial I}{\partial z}$ suffers a discontinuity at the maximum point of the function I at the interface, the term $\frac{\partial I}{\partial z}\frac{\partial \ln(\rho_e/r)}{\partial z}$ requires smoothing. As the result, we obtain an equation that gives an adequate solution at the interface between the media

$$\frac{\partial^2 I}{\partial r^2}+\frac{\partial^2 I}{\partial z^2}+\frac{\partial I}{\partial r}\frac{\partial \ln(\rho_e/r)}{\partial r}+\frac{\partial I}{\partial z}\left\{\frac{\partial}{\partial z}\left(\ln(\rho_e/r)\right)\right\}_{z\leq z_0-\varepsilon, z\geqslant z_0+\varepsilon}+\frac{\partial I}{\partial z}\left\{\frac{\partial P(\rho_e/r)}{\partial z}\right\}_{z_0-\varepsilon<z<z_0+\varepsilon}$$
$$=\frac{2\pi r}{\rho_e}\left(\frac{\partial S}{\partial r}\frac{\partial T}{\partial z}-\frac{\partial T}{\partial r}\left\{\frac{\partial S}{\partial z}\right\}_{z\neq z_0}-\frac{\partial T}{\partial r}\delta(z-z_0)[S]_{z=z_0}\right).$$

Here $P(\rho_e/r)$ is a cubic polynomial such that

$$\left(\frac{\partial^2 P(\rho_e/r)}{\partial z^2}\right)_{z=z_0\pm\varepsilon}=\left(\frac{\partial^2 \ln(\rho_e/r)}{\partial z^2}\right)_{z=z_0\pm\varepsilon}.$$

In the case of constant medium parameters considered, it is sufficient to use a sigmoid function for smoothing, which has the form

$$P(\rho_e/r)=\ln\left(\rho_e^{met}/r\right)\frac{1}{1-e^{z-z_0}}+\ln\left(\rho_e^{gas}/r\right),\quad \varepsilon=0.05\text{ mm}.$$

This regularization should serve as a starting point for further methodological investigations. For solving the complete system of Maxwell's equations (4) in the multidimensional case, numerical methods for solving electrodynamics problems with nonlinear effects that lead to significant changes in the characteristics of the electromagnetic field are known [20, 21]. For solving the simplified version of the system (4) in the form (5), both well-established iterative methods [22], finite element and finite volume methods [23, 24], as well as ready-made libraries [25] can be used. In the future, other economical methods [26, 27] is planned to be used for solving the problem. Solution of equation (4) by the method of successive over-relaxation (SOR) [28] at each time step allows us to build an efficient algorithm for the relaxation parameter $\omega=2-O(h)$ [29].

Let's increase the computational domain in the axial direction by a factor of two. We define grid function $T_{ik}=T(r_i,z_k)$, $I_{ik}^n=(I(r_i,z_k))^n$ on the grid nodes $r_i=ih$, $i=1,...,N_r$, $z_k=kh$, $k=1,...,2N_z$. At this stage, a stationary problem is solved using the value at a given time step where sufficiently high temperature values are reached. In the computational domain corresponding to the sample, the temperature obtained from the solution of the system (1) is set. In the region corresponding to the pair, a radial temperature distribution is specified on the surface $T_{ik}=T(r_i,N_z)$, $i=1,...,N_r$, $i=N_z+1,...,2N_z$. Let the grid functions lying on the line $z=z_0$ have indices $(i,N_z+1/2)$. Then, the

finite difference scheme for the system of equations (5) has the following form

$$\begin{cases} \Phi_{i,k} = \log(\rho_e(T_{i,k})/r_i), \quad i = 1, ..., N_r, \quad k = 1, ..., 2N_z, \\ ar_{i,k} = \frac{1}{4}\left(\ln(\rho_e/r)^n_{i+1,k} - \ln(\rho_e/r)^n_{i-1,k}\right), \\ az_{i,k} = \frac{1}{4}\left\{\ln(\rho_e/r)^n_{i,k+1} - \ln(\rho_e/r)^{n+1}_{i,k-1}\right\}_{k<k_0-l, k>k_0+l} \\ +\frac{1}{4}\left\{P_3(\rho_e/r)^n_{i,k+1} - P_3(\rho_e/r)^{n+1}_{i,k-1}\right\}_{k_0-l\le k\le k_0+l}, \\ F^n_{i,k} = \frac{1}{4}\frac{2\pi r_i}{\rho_e(T_{i,k})}\left((S(T_{i+1,k}) - S(T_{i-1,k}))(T_{i,k+1} - T_{i,k-1})\right. \\ \left. -(T_{i+1,k} - T_{i-1,k})(S(T_{i,k+1}) - S(T_{i,k-1}))\right)_{k<k_0-2, k>k_0+2} \\ -h(T_{i+1,k} - T_{i-1,k})\left(1 + \cos\left(\pi\frac{k-k_0}{2}\right)\right)(S(T_{i,k_0+1}) - S(T_{i,k_0}))_{k_0-2\le k\le k_0+2}\Big), \\ I^{n+1}_{i,k} = (1-\omega)I^n_{i,k} + \frac{\omega}{4}\left[I^{n+1}_{i-1,k}(1 - ar_{i,k}) + I^{n+1}_{i,k-1}(1 - az_{i,k})\right. \\ \left. +I^n_{i+1,k}(1 + ar_{i,k}) + I^n_{i,k+1}(1 + az_{i,k}) - F^n_{i,k}\right], \quad i = 2, ..., N_r - 1, \quad k = 2, ..., 2N_z - 1, \\ I_{i,1} = I_{1,k} = 0, \quad I_{i,2N_z} = I_{i,2N_z-1}, \quad I_{N_r,k} = I_{N_r-1,k}. \end{cases} \tag{7}$$

Along with other advantages, the SOR method is interesting from the viewpoint of the ease of implementation in cylindrical coordinates. The principle of expressing the desired element through the adjacent points of the "cross" type is universal and does not depend on the choice of the coordinate system. We can note that Eq. (5) and the solution algorithm contain division by radius only in the argument of the logarithm function in calculating $\Phi_{i,k}$. Since the logarithm function increases rather slowly as the argument grows, the division by quantities of order of $h/2$ does not lead to the appearance of the solution singularities while calculating in the vicinity of the symmetry axis.

4. COMPUTATION RESULTS

Let's solve problem (1) for constant and variable coefficients. As values, we will choose values close to the ones for temperatures above the melting temperature: $c(T) = 2.7 \times 10^8$, $\rho(T) = 1.6 \times 10^{-5}$, $\lambda(T) = 0.8 \times 10^{-1}$ for 6000 K. We will assume the melting heat L_m to be zero, excluding a phase transition. Lets consider problem (5) for the case when ρ_e, S are constant in the metal and in the gas. As values, we will choose values close to the ones for a temperature of 6000 K: $\rho_e^{met} = 1.5 \times 10^{-4}$, $\rho_e^{gas} = 0.7 \times 10^{-3}$, $S^{met} = 1.5 \times 10^{-5}$, $S^{gas} = 10^{-3}$.

Distribution for temperature and currents are received (see Fig. 3). Temperature distribution over the border $z = z_0$ repeats surface temperature, which is allowable assumption for a small vapor layer above the sample. The heating depth is very small, corresponding to the theory and is confirmed by comparison of calculated and experimental data [2]. Current distributions reach maximum values at $z = z_0$ sample border and propagate into gas and metal.

Let's compare the temperature profiles on the surface (Fig. 4a) obtained using constant coefficients without considering the phase transition and using coefficients that depend on temperature. Unlike the smooth solution obtained with constant coefficients, the full formulation of the Stefan problem solution produces a graph with singularities. The main contribution to the solution's shape comes from the thermal conductivity coefficient $\lambda(T)$, which enters the boundary condition in problem (1) and appears under the derivative terms with respect to space. The dependence $\lambda(T)$ experiences a discontinuity at the melting point and has different characteristics in the metal and the melt (Fig. 2b). Depending on the temperature profile on the surface, different solutions can be obtained at the interface between the media (see Fig. 4b). Despite the close values of the current amplitude, the current profile at the interface has a different nature. In the case of solving the complete Stefan problem, the current is non-uniformly distributed in the region, with high values concentrated outside the melt region. This is because the source of the current is not the temperature itself but the temperature difference, similar to a thermocouple that does not generate energy when the entire system is uniformly heated. At the same time, the current locally closes since the principle of superposition applies in this problem: current arises from each surface segment independently and decays in a power-law manner. Therefore, the details of heating strongly influence the current distribution pattern.

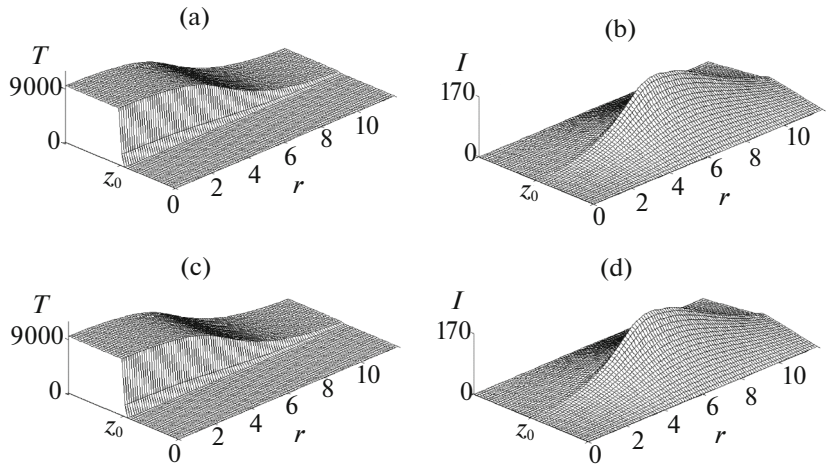

Fig. 3. The temperature distribution (a, c) and corresponding current distribution (b, d) at sample cross section.

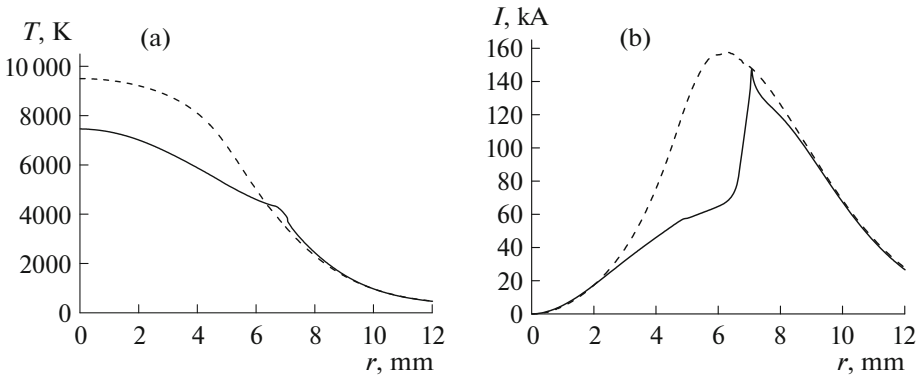

Fig. 4. Plots of radial temperature distribution (a) and the corresponding current (b) on the plate's surface. The results of the Stefan problem calculation with variable coefficients (solid line) and constant coefficients (dashed line).

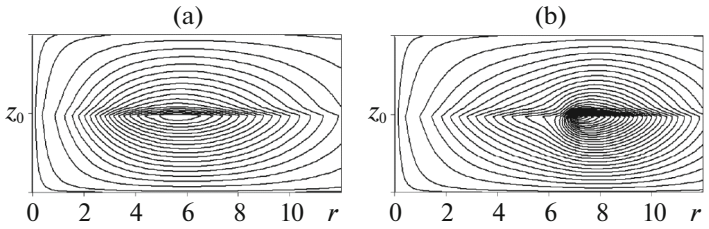

Fig. 5. Distribution of the radial component of the current on the transverse section of the plate and the region above it for constant coefficients (a) and variable coefficients (b) of the Stefan problem.

The closed contour lines of thermal currents (see Fig. 5) change their nature. A smooth temperature profile on the surface produces nearly symmetric contour lines with respect to the sample's surface at $z = z_0$. In the absence of smoothness in the derivative of temperature with respect to the radius, shifted current lines are obtained because at the center of the heated surface, the temperature distribution is sufficiently smooth and there is no local source of closed currents. The change in the bending nature near the boundary is due to the radius of smoothing used for the discontinuous functions. After replacing the sigmoid function with a cubic polynomial with carefully selected coefficients, these non-physical features of the solution will disappear. The calculation results will serve as a basis for introducing variable coefficients into the solution of problem (5), which will undoubtedly change the position of the current amplitude maximum and complicate the contour lines' pattern.

5. CONCLUSIONS

Modeling of thermal currents arising from pulsed heating of a tungsten plate and a thin layer of vapor has been conducted based on solving the equations of electrodynamics in the sample region and above it. The temperature in the sample region is obtained by solving a two-phase Stefan problem in a cylindrical coordinate system. A model temperature distribution of evaporating tungsten is used, which replicates the surface temperature, corresponding to the physics of the process in the considered thin vapor layer. The case of constant values of electrical resistance and thermoelectric power in the gas and metal is considered. The results of the modeling demonstrate that the detailed consideration of the Stefan problem coefficients has a significant influence on the results of the electrodynamics equation solution. Further development of the model involves refining the calculation of the gas's specific electrical conductivity, the metal's thermoelectric power, and incorporating numerical calculations of temperature and gas density.

FUNDING

This work has been supported by the grants the Russian Science Foundation no. 23-21-00134.

CONFLICT OF INTEREST

The authors of this work declare that they have no conflicts of interest.

REFERENCES

1. L. Vyacheslavov, A. Arakcheev, A. Burdakov, I. Kandaurov, A. Kasatov, V. Kurkuchekov, K. Mekler, V. Popov, A. Shoshin, D. Skovorodin, Y. Trunev, and A. Vasilyev, "Novel electron beam based test facility for observation of dynamics of tungsten erosion under intense ELM-like heat loads," AIP Conf. Proc. **1771**, 060004 (2016).
2. A. S. Arakcheev, D. E. Apushkinskaya, I. V. Kandaurov, A. A. Kasatov, V. V. Kurkuchekov, G. G. Lazareva, A. G. Maksimova, V. A. Popov, V. Snytnikov, Yu. A. Trunev, A. A. Vasilyev, and L. N. Vyacheslavov, "Two-dimensional numerical simulation of tungsten melting under pulsed electron beam," Fusion Eng. Des. **132**, 13–17 (2018).
3. G. G. Lazareva, V. A. Popov, A. S. Arakcheev, A. V. Burdakov, I. V. Shwab, V. L. Vaskevich, A. G. Maksimova, N. E. Ivashin, and I. P. Oksogoeva, "Mathematical simulation of the distribution of the electron beam current during pulsed heating of a metal target," J. Appl. Ind. Math. **24**, 97–108 (2021).
4. V. A. Popov, A. S. Arakcheev, I. V. Kandaurov, A. A. Kasatov, V. V. Kurkuchekov, Yu. A. Trunev, A. A. Vasilyev, and L. N. Vyacheslavov, "Theoretical simulation of the closed currents near non-uniformly strongly heated surface of tungsten due to thermo-emf," Phys. Plasmas **29**, 033503 (2022).
5. G. G. Lazareva, A. S. Arakcheev, A. A. Vasilyev, and A. G. Maksimova, "Numerical simulation of tungsten melting under fusion reactor-relevant high-power pulsed heating," Smart Innov. Syst. Technol. **133**, 41–51 (2019).
6. J. W. Davis and P. D. Smith, "ITER material properties handbook," J. Nucl. Mater. **233**, 1593–1596 (1996).
7. C. Y. Ho, R. W. Powell, and P. E. Liley, "Thermal conductivity of elements," J. Phys. Chem. Ref. Data **279** (1972).
8. G. Pottlacher, "Thermal conductivity of pulse-heated liquid metals at melting and in the liquid phase," J. Non-Cryst. Solids **250**, 177–181 (1999).
9. G. G. Lazareva, A. S. Arakcheev, A. G. Maksimova, and V. A. Popov, "Numerical model of evaporation of tungsten in vacuum under high-power transient heating," J. Phys.: Conf. Ser. **1391**, 012074 (2019).
10. G. G. Lazareva and A. G. Maksimova, "Numerical simulation of the propagation of tungsten vapor above a heated surface," J. Appl. Ind. Math. **16**, 472–480 (2022).
11. J. D. Jackson, *Classical Electrodynamics,* 3rd ed. (Wiley, New York, 1999).
12. H. Buchholz, *Elektrische und Magnetische Potentialfelder* (Springer, Berlin, 1957).
13. W. Smythe, *Static and Dynamic Electricity* (McGraw-Hill, New York, 1967).
14. A. A. Samarsky and P. N. Vabishevich, *Computational Heat Transfer,* 2nd ed. (Librokom, Moscow, 2009) [in Russian].
15. A. A. Samarsky and B. D. Moiseenko, "An economic continuous calculation scheme for the stefan multidimensional problem," USSR Comput. Math. Math. Phys. **5** (5), 43–58 (1965).
16. V. A. Popov, A. S. Arakcheev, A. V. Burdakov, A. A. Kasatov, A. A. Vasilyev, and L. N. Vyacheslavov, "Theoretical modeling of shielding for plasma flow and electron beam heating," AIP Conf. Proc. **1771**, 060009 (2016).

17. J. Douglas and H. H. Rachford, "On the numerical solution of heat conduction problems in two and three space variables," Trans. Am. Math. Soc. **82**, 421–439 (1956).
18. V. T. Zhukov and O. B. Feodoritova, "On development of parallel algorithms for solving parabolic and elliptic equations," J. Math. Sci. **254**, 606–624 (2021).
19. J. Waldén, "On the approximation of singular source terms in differential equations," Numer. Methods Part. Differ. Equat. **15**, 503–520 (1999).
20. V. P. Zagonov, "Mathematical modeling of electromagnetic impact of pulsed fields on complex technical systems," in *Functioning and Development of Complex National Economic, Technical, Energy, Transport Systems, Communication Systems and Communications* (MGF Znanie, Moscow, 1998), pp. 392–394 [in Russian].
21. M. E. Zhukovskii, "Self-consistent quasi-3D model of radiation excitation of electromagnetic fields," Mat. Model. **8** (4), 3–20 (1996).
22. V. M. Sadovskii and O. V. Sadovskaya, "Mathematical modeling of inhomogeneous electric field impact on a liquid crystal layer," Zeitschr. Angew. Math. Mech. (2022).
23. J. Droniou, "Finite volume schemes for diffusion equations: Introduction to and review of modern methods," Math. Models Methods Appl. Sci. **24**, 1575–1619 (2014).
24. Y. Vassilevski, K. Terekhov, K. Nikitin, and I. Kapyrin, *Parallel Finite Volume Computation on General Meshes* (Springer Int., Cham, 2020).
25. I. Kulikov, I. Chernykh, and A. Tutukov, "A new hydrodynamic code with explicit vectorization instructions optimizations that is dedicated to the numerical simulation of astrophysical gas flow, numerical method, tests, and model problems," Astrophys. J. Suppl. Ser. **243** (1) (2019).
26. S. C. Eisenstat, H. C. Elman, and M. H. Schultz, "Variational iterative methods for nonsymmetric systems of linear equations," SIAM J. Numer. Anal. **20**, 345–357 (1983).
27. P. Benedusi, G. Janett, L. Belluzzi, and R. Krause, "Numerical solutions to linear transfer problems of polarized radiation," Astron. Astrophys. **655**, A88 (2021).
28. A. A. Samarskii and E. S. Nikolaev, *Methods of Solution of Grid Equations* (Fizmatgiz, Moscow, 1978) [in Russian].
29. R. G. Strongin, V. P. Gergel, V. A. Grishagin, and K. A. Barkalov, *Parallel Computing in Problems of Global Optimization* (Mosk. Gos. Univ., Moscow, 2013) [in Russian].